

Zebularine induces enzymatic DNA–protein crosslinks in 45S rDNA heterochromatin of *Arabidopsis* nuclei

Klara Prochazkova^{1,†}, Andreas Finke^{2,†}, Eva Dvořák Tomašíková¹, Jaroslav Filo¹, Heinrich Bente^{1,2}, Petr Dvořák³, Miroslav Ovečka⁴, Jozef Šamaj⁴ and Ales Pecinka^{1,2,5,*}

¹Institute of Experimental Botany, The Czech Academy of Sciences, Centre of the Region Haná for Biotechnological and Agricultural Research, Šlechtitelů 31, 77900 Olomouc, Czech Republic, ²Max Planck Institute for Plant Breeding Research, Carl-von-Linné-Weg 10, 50829 Cologne, Germany, ³Department of Botany, Faculty of Science, Palacký University Olomouc, Šlechtitelů 27, 78371 Olomouc, Czech Republic, ⁴Department of Cell Biology, Centre of the Region Haná for Biotechnological and Agricultural Research, Faculty of Science, Palacký University Olomouc, Šlechtitelů 27, 78371 Olomouc, Czech Republic and ⁵Department of Cell Biology and Genetics, Faculty of Science, Palacký University, Šlechtitelů 27, 78371 Olomouc, Czech Republic

Received November 05, 2021; Editorial Decision November 23, 2021; Accepted December 01, 2021

ABSTRACT

Loss of genome stability leads to reduced fitness, fertility and a high mutation rate. Therefore, the genome is guarded by the pathways monitoring its integrity and neutralizing DNA lesions. To analyze the mechanism of DNA damage induction by cytidine analog zebularine, we performed a forward-directed suppressor genetic screen in the background of *Arabidopsis thaliana* zebularine-hypersensitive *structural maintenance of chromosomes 6b (smc6b)* mutant. We show that *smc6b* hypersensitivity was suppressed by the mutations in *EQUILIBRATIVE NUCLEOSIDE TRANSPORTER 3 (ENT3)*, *DNA METHYLTRANSFERASE 1 (MET1)* and *DECREASE IN DNA METHYLATION 1 (DDM1)*. Superior resistance of *ent3* plants to zebularine indicated that ENT3 is likely necessary for the import of the drug to the cells. Identification of MET1 and DDM1 suggested that zebularine induces DNA damage by interference with the maintenance of CG DNA methylation. The same holds for structurally similar compounds 5-azacytidine and 2-deoxy-5-azacytidine. Based on our genetic and biochemical data, we propose that zebularine induces enzymatic DNA–protein crosslinks (DPCs) of MET1 and zebularine-containing DNA in *Arabidopsis*, which was confirmed by native chromatin immunoprecipitation experiments. Moreover,

zebularine-induced DPCs accumulate preferentially in 45S rDNA chromocenters in a DDM1-dependent manner. These findings open a new avenue for studying genome stability and DPC repair in plants.

INTRODUCTION

Genome stability is constantly challenged by manifold external and internal factors (1). To minimize the risk of mutations, organisms have evolved dedicated DNA repair pathways that remove various types of lesions from the genome (2). Well-known lesions include DNA strand breaks, mismatched nucleotides, damaged bases or nucleotides, and intra- or interstrand crosslinks. Recently, a novel repair pathway involved in the removal of DNA–protein crosslinks (DPCs) has been described in fungi and animals (3). At least some of its components are conserved also in plants (4,5). DPCs are formed by proteins covalently attached to DNA molecules (6). Because DPCs represent a barrier for the movement of DNA-associated enzymes, they are recognized as abnormal structures and trigger DNA damage signaling and repair (7). DPCs are probably one of the most variable types of DNA damage owing to the different sizes and structures of the attached proteins, types of bonds and a variety of modes of action of the crosslinking agents. The general crosslinkers, such as formaldehyde, induce the so-called nonenzymatic DPCs between DNA and any associated protein. In contrast, specific poisons promote or stabilize the binding of a given enzyme to DNA and induce the so-called enzymatic DPCs. The list of poten-

*To whom correspondence should be addressed. Tel: +420 585 238 709; Email: pecinka@ueb.cas.cz

[†]The authors wish it to be known that, in their opinion, the first two authors should be regarded as Joint First Authors.

Present addresses:

Andreas Finke, Hamilton Bonaduz AG, Application Laboratory, CH-4123 Allschwil, Switzerland.

Heinrich Bente, Department of Plant Biology, Swedish University of Agricultural Sciences and Linnean Center for Plant Biology, 75007 Uppsala, Sweden.

tial DPC inducers is still growing, and finding new types of crosslinking agents may reveal new molecular components and their repair pathways.

Methylation of cytosine at the fifth position of the aromatic ring (5-methylcytosine, 5mC, DNA methylation) is an important epigenetic regulatory mark occurring in CG, CHG and CHH (where H is A, T or C) nucleotide sequence contexts in plants (8). All types of DNA methylation can be established *de novo* by the DOMAINS REARRANGED METHYLTRANSFERASEs within the RNA-directed DNA methylation pathway (9). Existing CG and CHG methylation patterns are then perpetuated by DNA METHYLTRANSFERASE 1 (MET1) and CHROMOMETHYLASE 3 (CMT3), respectively (10,11). MET1 and CMT3 genetically interact with the SWI/SNF2-type chromatin remodeler DECREASE IN DNA METHYLATION 1 (DDM1) to maintain DNA methylation at repetitive sequences (11).

In plants, DNA methylation is removed by shutting down the replication-coupled DNA methylation machinery or by the activity of 5mC-dependent DNA glycosylases (12). Additionally, several chemical compounds transiently reducing DNA methylation have been identified (13). Dihydroxypropyladenine and 3-deazaneplanocin A inhibit the activity of *S*-ADENOSYL-L-HOMOCYSTEINE HYDROLASE 1, thus reducing the synthesis of the methyl group and leading to an overall reduction in DNA and histone methylation (14,15). In contrast, nonmethylable cytidine analogs from the 5-azacytidine group, including 5-azacytidine (AC), 2-deoxy-5-azacytidine (DAC) or zebularine, target primarily DNA methylation (16,17). After incorporation, the nucleoside analogs change the interaction between DNA and DNMTs (18). Under normal conditions, the methyl group is transferred from the cofactor *S*-adenosyl methionine, resulting in formation of 5mC and release of the DNMT by β -elimination. Incorporation of the nucleotide analogs prevents the β -elimination, resulting in a covalent complex. The DNMT remains bound to the DNA.

Also, zebularine, AC and DAC induce genome stress. While this effect was described already in the early studies using bacteria and fungi (19–22), it was neglected by the plant community. Only recently, few studies using *Arabidopsis* and cereals showed that these drugs activate DNA damage signaling, trigger genome instability and are highly toxic for specific DNA damage repair mutants (23–25). In particular, structural maintenance of chromosomes 5/6 (SMC5/6) subunits STRUCTURAL MAINTENANCE OF CHROMOSOMES 6B (SMC6B) and NON-SMC ELEMENT 4A were found to be important for the repair of zebularine-induced DNA damage as demonstrated by a strong hypersensitivity of their loss-of-function mutants to this drug (24,26). At the same time, the nature of DNA damage induced by zebularine treatment remained unknown. This hampered a more targeted use of cytidine analogs in plant DNA damage repair studies.

To identify the zebularine-induced DNA damage, we set up a forward-directed suppressor screen using the zebularine-hypersensitive genetic background of *Arabidopsis smc6b-1* mutant. The screen was named ZEBULARINE-RESISTANT *smc6b* (ZRS) and the identified suppressor mutants corresponded to five complementation groups

(ZRS1–5), out of which ZRS1, ZRS2 and ZRS4 are described here.

MATERIALS AND METHODS

Plant materials, growth conditions and drug treatments

Arabidopsis thaliana wild type (WT) and mutants in Col-0 background (unless stated otherwise) were used in this study: *smc6b-1* (SALK_123114C), *ent3-1* (SALK_131585), heterozygous *met1-3* (27), *cmt3* (splice acceptor mutation located in the intron 11, in Ws-2 background) (28) and *ddm1-5* (82-bp insertion in the exon 2; the original mutant was produced in Zurich background, but we used its backcross to Col-0) (29). We used two reporter lines MET1-RFP (30) and PCNA1-GFP (31) in Col-0 background. All lines were used as homozygotes, unless stated otherwise.

For cultivation in soil, seeds were spread on tap water-soaked substrate, covered with a transparent plastic cup to maintain high humidity and placed in an air-conditioned phytochamber with a long-day regime (16 h light, 150 $\mu\text{mol m}^{-2} \text{s}^{-1}$, 21°C, 8 h dark, 19°C). Two-leaf stage plants were singled into individual 7 \times 7 cm² pots and grown at the same condition until maturity.

For cultivation *in vitro*, seeds were surface sterilized with 70% ethanol and 8% hypochlorite and stratified for 2–3 days. Seeds were evenly spread on half-strength Murashige and Skoog ($\frac{1}{2}$ MS) medium with 0.6% phyto agar (Duchefa Biochemie) and with or without the addition of zebularine (Sellekchem, Sigma-Aldrich), AC, DAC, 5-fluorouridine (5-FUrd), mitomycin C (all Sigma-Aldrich) or bleocin (Calbiochem). Applied drug concentrations are specified in the text.

For root length assays, plants were germinated and grown continuously on mock or drug-containing solid media for 8 days. Subsequently, the plants were carefully pulled out of agar, stretched and the length of the primary root was measured manually.

The experiments were done with all available alleles of given mutant and a single set of controls. Due to space reasons, these experiments were divided between the main figures and supplementary figures. These pairs of figures contain duplicated images and quantitative data for the controls.

Forward-directed genetic screen and mapping by sequencing

For the ZRS genetic screen (Supplementary Figure S1), ~10 000 seeds of *smc6b-1* were imbibed in 0.1% KCl and agitated at 4°C for 8 h, and then seeds were washed with distilled water and incubated in 0.2% (v/v) watery ethyl methanesulfonate (EMS) solution at room temperature for 12 h to induce mutations. Afterward, seeds were washed 2 \times 5 min with 100 mM sodium thiosulfate and 3 \times 5 min with water. Finally, the seeds were suspended in 0.1% agarose and spread on the soil surface at a density of ~100 seeds per 18 \times 14 cm² tray. The M₁ plants were grown until maturity and seeds of all plants from one tray were collected together resulting in 100 M₂ seed batches. Approximately 1500 seeds per batch were sterilized using 8% sodium hypochlorite solution for 6–8 min, washed with 70%

ethanol for 5 min, rinsed with sterile water, mixed with 0.1% agarose and spread on the plates with sterile $\frac{1}{2}$ MS media supplemented with 20 μ M zebularine. Internal zebularine-sensitive *smc6b-1* and resistant WT controls were included in every plate. The plants were grown in a phytochamber under long-day conditions for 10 days. Afterward, the plates were inspected and the primary mutant candidates showing more vigorous root and/or shoot growth than *smc6b-1* were transferred to soil and grown until maturity. The M₃ plants were grown on 20 μ M zebularine- or 50 μ M 5-FUrd-containing $\frac{1}{2}$ MS media to confirm M₂ phenotypes and identify the drug uptake mutants, respectively. To exclude the *SMC6B* allele contamination, every zebularine-resistant candidate was tested for *smc6b-1* homozygosity by PCR.

The candidates selected for mapping were backcrossed to the nonmutagenized *smc6b-1* and their BCF₂ population was screened on 20 μ M zebularine-containing $\frac{1}{2}$ MS media. Segregation of the zebularine-resistant phenotype was assessed and it typically matched the segregation pattern for a single recessive locus. About 75–150 zebularine-resistant plants were collected, pooled and their genomic DNA was isolated using Nucleon PhytoPure kit (GE Healthcare). Genomic DNA was sonicated into 350-bp fragments by a Covaris device and cloned into the DNA TruSeq-type (Illumina) library. The library quality was assessed using Bioanalyzer (Agilent) and the library was sequenced as single-end or paired-end protocol on a HiSeq2500 instrument (Illumina) to $\sim 35\times$ genome coverage. Sequencing data were further analyzed using bioinformatics tools available at the public platform usegalaxy.org version 19.01 (Supplementary Figure S2). The reads were mapped to the *A. thaliana* reference genome (TAIR10) with bowtie2 version 2.4.2 in default settings (32,33). Read sorting, SNP calling and filtering were done using tools from the MiModD version 0.1.9 tool set (<https://celegans.de/mimodd/>) and annotated with SnpEff tool version 4.3 (34). All tools of MiModD were used by default settings, except MiModD VCF filter where indels were excluded. For annotation via SnpEff, all possibilities of information were used.

RNA isolation, cDNA synthesis and qPCR

RNA was extracted using the RNeasy kit (Qiagen) with on-column DNase I (Thermo Fisher Scientific) treatment. The purity of the isolated RNA was monitored using cDNA reaction without reverse transcriptase (RT) by PCR. cDNA for analysis of splice acceptor (*zrs2-1*) mutation was synthesized from 1 μ g of total RNA per sample with RevertAid H-Minus First-Strand Synthesis Kit using oligo-d(T) primers (Thermo Fisher Scientific). The region was amplified from cDNA using primers specific for the 11th and 14th exons of *ZRS2*. The amplified DNA was purified from the 2% agarose gel with QIAquick gel extraction kit (Qiagen) and sequenced using the Sanger method with primers listed in Supplementary Table S2. The sequence analysis was performed in SnapGene 5.2.

For analyses of *MET1* steady-state transcript amount, 100 mg of 5-day-old mock- and 24-h 40 μ M zebularine-treated seedlings were harvested in liquid nitrogen. Total RNA extraction and cDNA synthesis were performed as

described earlier. cDNA was diluted 1:5 and RT-qPCR was performed using 2 μ l of cDNA per 20 μ l reaction with the 5 \times HOT FIREPol Eva Green qPCR Mix Plus (ROX) kit (Solis Biotec) on a CFX96 Touch Real-Time PCR Detection System (Bio-Rad). Fold changes were calculated relative to mock-treated control using the standard curve method. qPCR experiments were performed following the MIQE guidelines (35). Experiment was performed in three biological replicates for each of three technical replicates. *PP2A* (AT1G69960) was used as the reference gene. Primers used in this study are listed in Supplementary Table S2.

Root length and cotyledon area measurements

Eight-day-old seedlings grown on control or drug-containing media were carefully pulled out from agar using tweezers and stretched on fresh agar plates. Plants with stretched roots were photographed with a D5600 (Nikon) digital camera with 80-mm Nikkor objective and their root length was measured using ImageJ calibrated with internal size control. Roots of at least 15 plants per genotype and treatment were measured in one replicate and at least three biological replicates were performed. For cotyledon area measurements, seedlings were photographed right on the plates from the top view and measured in ImageJ as described earlier.

Cell death assays

Seeds were grown on vertically positioned plates with $\frac{1}{2}$ MS medium for 5 days, and then transferred to liquid $\frac{1}{2}$ MS media without (mock) and with 20 μ M zebularine, 20 μ M AC, or 20 or 10 μ M DAC for another 2 days. Subsequently, the seedlings were stained with 10 mg ml⁻¹ of propidium iodide (PI) solution (Sigma) for 3 min, followed by a rinsing step with sterilized water. Then, they were placed on slides in a drop of water and analyzed using a Zeiss AxioImager Z2 microscope (Zeiss, Oberkochen, Germany) equipped with a high-performance DSD2 confocal module (Andor) and Plan-APOCHROMAT 10 \times /0.45 objective. Representative phenotypes were imaged with a Leica confocal microscope TCS SP8 (Leica, Wetzlar, Germany) and HC PL APO CS2 20 \times /0.75 DRY objective equipped by Leica LAS-X software with a Leica Lightning module laser scanning confocal microscope (Leica).

Live-cell microscopy

Seeds were germinated on vertically positioned plates with $\frac{1}{2}$ MS medium for 3–4 days, and then the seedlings were placed into an adaptation chamber prepared as described (36). Microscopic slides and coverslips were cleaned by dish soap and washed subsequently with copious amounts of distilled water, 70% ethanol and distilled water again. The slides were air-dried and placed into the Coplin jar with 96% ethanol for 20 min. The slides were air-dried under sterile conditions and on each slide two thin stripes of parafilm were placed at a distance of ~ 18 mm. The seedling was placed into a 10- μ l droplet of liquid $\frac{1}{2}$ MS and covered by coverslip reaching parafilm on its edges in a way that leaves

stayed outside of the chamber. The slides were then placed vertically into the Coplin jar filled with liquid $\frac{1}{2}$ MS to the level reaching hypocotyls and the seedlings were adapted for 10–12 h. The next day, the mock and drug treatment was performed using perfusion for exchange of the media (36). The concentrations of DNA damaging drugs are specified in the ‘Results’ section. After 2 h of incubation, the samples were analyzed. The analyses were performed using a Cell Axio Observer Z1 spinning disk confocal microscope (Zeiss) with objective EC-Plan-Neofluar 40 \times /1.30 Oil DIC M27 suitable for live-cell microscopy (37).

For analyses of MET1 in *ddm1* background, *ddm1* MET1-RFP and MET1-RFP plants were grown as stated earlier. Five-day-old seedlings were treated with 40 μ M zebularine and analyzed at 8 and 24 h after the treatment. Plants were analyzed with a Leica confocal microscope TCS SP8 (Leica, Wetzlar, Germany) and HC PL APO CS2 20 \times /0.75 DRY objective equipped by Leica LAS-X software with a Leica Lightning module laser scanning confocal microscope (Leica).

Southern analysis using methylation-sensitive restriction enzymes

For Southern analysis, genomic DNA was isolated with the modified Dellaporta method (38). Approximately 500 ng of gDNA was digested with HpaII or MspI (Thermo Fisher Scientific) overnight at 37°C. The digested DNA was separated overnight on 1.2% Tris–borate–EDTA agarose gel, depurinated, denatured and neutralized as described (17). The gels were blotted onto Hybond N+ (Amersham) membranes for 6 h with 20 \times and 2 \times SSC gradient. Membranes were washed with 2 \times SSC, air-dried and UV-crosslinked using a Stratelinker (Stratagene). Hybridization was performed according to the protocol (39) with modifications as described (25). Blotted DNA was detected with biotin-labeled probes specific for *Arabidopsis* centromeric repeat *pAL* and *5S rDNA* repeat using Chemiluminescent Nucleic Acid Detection Module Kit (Thermo Fisher Scientific; 89880) by following the manufacturer’s instructions.

Flow cytometry

The somatic ploidy was analyzed by flow cytometry. One or two leaves from 14-day-old seedlings were chopped with a razor blade in 500 μ l Otto I solution [0.1 M citric acid, 0.5% (v/v) Tween 20] to prepare a nuclear suspension. The suspension was filtered through 50- μ m nylon mesh and stained with 1 ml of Otto II solution (0.4 M Na₂HPO₄·12H₂O) containing 20 μ g ml⁻¹ DAPI (4',6-diamidino-2-phenylindole). The ploidy was analyzed on a Partec PAS I flow cytometer using a diploid WT *Arabidopsis* as an internal control.

DNMT protein alignment

Multiple sequence alignment was performed to elucidate the conservation level of mutations in *ZRS4*. Sequences of *A. thaliana* (P34881), *Medicago truncatula* (G7KP96), *Solanum lycopersicum* (O49889), *Brachypodium distachyon* (DNMT1a: A0A0Q3RHH0; DNMT1b:

A0A0Q3LBT8), *Zea mays* (DNMT1b-0: A0A3L6DXI1; DNMT1b-1: A0A3L6DYY8), *Oryza sativa* (DNMT1a: Q7Y1I7; DNMT1b: B1Q3J6), *Homo sapiens* (P26358), *Mus musculus* (P13864), *Rattus norvegicus* (Q9Z330) and *Gallus gallus* (Q92072) were retrieved from UniProt (<https://www.uniprot.org/>) and analyzed using tool ClustalW in the program MEGA-X (Molecular Evolutionary Genetics Analysis) (40).

ImmunoFISH

For immunoFISH, 5-day-old seedlings were incubated in mock and 40 μ M zebularine for 24 h. Seedlings were fixed with 4% formaldehyde in Tris buffer (10 mM Tris–HCl, pH 7.5, 10 mM NaEDTA and 100 mM NaCl) at 4°C for 20 min and washed 2 \times 10 min with Tris buffer at 4°C. They were chopped in 500 μ l LB01 buffer (15 mM Tris–HCl, pH 7.5, 2 mM NaEDTA, 0.5 mM spermine, 80 mM KCl, 20 mM NaCl and 0.1% Triton X-100) and filtered through 50- and 20- μ m cell strainer caps. RFP-positive nuclei were sorted on the slides by FACSaria (Becton Dickinson) flow sorter in sorting buffer (100 mM Tris–HCl, pH 7.5, 50 mM KCl, 2 mM MgCl₂, 0.05% Tween 20 and 5% sucrose). Around 3000 nuclei were sorted per slide. Slides were post-fixed with 4% formaldehyde in phosphate-buffered saline (PBS) for 15 min and washed with PBS. For immunolocalization of MET1-RFP, slides were incubated with the rabbit anti-RFP primary antibody diluted 1:500 (600-401-379, Rockland Antibodies & Assays) at 4°C overnight and the secondary goat anti-rabbit Alexa Fluor 546 diluted 1:250 (A11003, Invitrogen) at room temperature for 2 h. Before FISH, slides were fixed in 3:1 ethanol/acetic acid for 10 min, followed by 10-min fixation in 3.7% formaldehyde in PBS. Slides were washed with PBS. FISH probes specific for *5S rDNA*, *45S rDNA* and centromeric repeat (*pAL*) were amplified from *A. thaliana* Col-0 genomic DNA and directly labeled with biotin-dUTP or digoxigenin-dUTP (Roche) during PCR. Slide pretreatment, hybridization, post-hybridization washes and detection were carried out as described (41,42). Biotin-dUTP was detected by goat anti-avidin conjugated with biotin (1:100, Vector Laboratories) and avidin combined with Texas Red (1:1000, Vector Laboratories), digoxigenin-dUTP by mouse anti-digoxigenin (1:250, Roche) and goat anti-mouse conjugated with Alexa Fluor 488 (1:200, Molecular Probes).

Subsequently, the slides were shortly washed with 1 \times PBS, nuclei were counterstained with DAPI (300 ng μ l⁻¹) and mounted in Vectashield (H-1000, Vector Laboratories). Imaging was performed with a Leica confocal microscope TCS SP8 (Leica 265 Microsystems) and HC PL PAO CS2 63 \times /1.4 OIL objective equipped by Leica LAS-X software (Leica). Images were captured separately for each fluorochrome, by using 546 (Alexa Fluor 546), 594 (Texas Red), 488 (Alexa Fluor 488) and 405 (DAPI) nm laser lines for excitation and appropriate emission filters. Processing of the final image was done in Imaris (Bitplane) and Adobe Photoshop version 6.0 (Adobe Systems Corporation, San Jose, CA). The quantitative analysis of MET1-RFP colocalization with H3K9me₂, *pAL*, *45S* and *5S rDNA* was performed in FIJI using fluorescent intensity profile for both correlated signals. The respective colocalization coefficients

were calculated by Pearson's correlation coefficient in Microsoft Excel.

Native chromatin immunoprecipitation–quantitative PCR assays

For native chromatin immunoprecipitation (N-ChIP), 5-day-old seedlings were incubated in mock and 40 μ M zebularine for 24 h. About 250 seedlings from two independent biological replicates were frozen in liquid nitrogen and were used for crude nuclei extraction for ChIP experiments as previously described without crosslinking with formaldehyde (43,44). Antibody against RFP raised in rabbit (600-401-379, Rockland Antibodies & Assays) was used for ChIP. To examine the accumulation of MET1-RFP at the target loci, primers against 5S rDNA and 45S rDNA were used. Samples were normalized to input DNA prepared from each chromatin preparation. qPCR was performed in three technical replicates for each biological replicate. Biological replicates are shown as mean of technical replicates and standard error represents variation of the technical replicates. Primers used for N-ChIP–qPCR are shown in Supplementary Table S2.

Statistical analyses

Statistical analyses were performed in the program Minitab 18 using 'one-way' ANOVA and post-hoc Tukey's test with the interval of probability $P < 0.05$. Statistical significance of MET1 RT-qPCR and ChIP experiments was evaluated with the Student's *t*-test in Microsoft Excel.

RESULTS

ZRS1 is a nucleoside transporter required for zebularine uptake

Treatment with 10 μ M zebularine causes 34% and 93% reduction in root length of WT and *smc6b-1* plants relative to the mock treatment of the same genotype, respectively (Figure 1A and B). The strong root growth reduction in *smc6b-1* is accompanied by cell death in the root meristem (Figure 1C). To identify the zebularine-hypersensitive suppressor mutants, we set up a forward-directed genetic screen (Supplementary Figure S1). Seeds of zebularine-hypersensitive homozygous *smc6b-1* plants (24,25) were EMS mutagenized, and the M₂ plants were screened for more vigorous root and/or shoot growth on 20 μ M zebularine-containing media. The validation and subsequent experiments were carried out with 10 μ M zebularine concentration. The first candidate showed greatly improved root growth (112.5%, Tukey's test, $P < 0.05$), indicating a complete lack of zebularine hypersensitivity (Figure 1A and B), and was named *zebularine-resistant smc6b 1 (zrs1)*. The next candidate *smc6b-1 zrs1-2* showed a very similar phenotype (Supplementary Figure S3A–C), and complementation crossing revealed that it is allelic to *smc6b-1 zrs1-1* (not shown).

To identify the causal gene, we performed mapping by sequencing (MBS) using a pool of \sim 100 BCF₂ zebularine-resistant plants (Supplementary Figure S2). Both *zrs1-1* and

zrs1-2 mutations were located at the top arm of chromosome 4 (Supplementary Figure S3D and E). Within this region, both *smc6b-1 zrs1-1* and *smc6b-1 zrs1-2* lines carried G→A transitions resulting in G183R and G281R substitutions in *ENT3* (At4g05120), respectively (Figure 1D; Supplementary Figures S4 and S5). *ENT3* is a known nucleoside transporter, and its mutant *ent3-1* showed resistance to a highly toxic pyrimidine analog 5-FUrd in *Arabidopsis* (45). Therefore, we performed a sensitivity assay using 50 μ M 5-FUrd, which revealed the lethality of WT and *smc6b-1* plants, while *smc6b-1 zrs1-1* and *smc6b-1 zrs1-2* plants continued vigorously growing (Figure 1A and B; Supplementary Figure S3A–C). To reveal whether there are other *ZRS1* mutants in our collection, we analyzed phenotypes of the remaining (in the meantime selected) *smc6b-1 zrs* candidates and found five additional 5-FUrd-resistant lines (Figure 1A–D; Supplementary Figure S3A–C). Sequencing of *ENT3* in these lines revealed additional point mutations leading to nonsynonymous amino acid substitutions (Figure 1D; Supplementary Table S1). To validate *ENT3* as our candidate, we used a characterized T-DNA insertional mutant *ent3-1* (45) and produced double homozygous *smc6b-1 ent3-1* plants. These plants showed full resistance to 10 μ M zebularine and 50 μ M 5-FUrd (Figure 1A and B). Therefore, we conclude that *ZRS1* is allelic to *ENT3*. The predicted function of *ENT3* is nucleoside transport through the plasma membrane (45). Analysis of roots of *smc6b-1 zrs1-1*, *smc6b-1 zrs1-3* and *smc6b-1 ent3-1* plants revealed complete suppression of the cell death phenotype upon zebularine treatment (Figure 1C), indicating a complete absence of zebularine-induced DNA damage in cell nuclei of *zrs1/ent3* mutants.

Identification of *ZRS1/ENT3* raised the question of whether it transports also other cytidine analogs of the AC family. Therefore, we treated the controls and all *smc6b-1 zrs1/ent3-1* genotypes with 10 μ M AC and 5 μ M DAC (Supplementary Figure S6). WT plants showed almost normal root length after our AC treatment (5.6% reduction) but had strongly reduced root length (by 77.3%) after treatment with more toxic DAC. *smc6b-1* plants were hypersensitive to AC and even more to DAC (15% and 6.4% root length compared to mock, respectively). In contrast, *smc6b-1 zrs1/ent3-1* double mutants showed significantly improved root growth after exposure to both drugs (77.9–130.5% root length compared to mock-treated WT; Tukey's test, $P < 0.05$). Also, the *smc6b-1 zrs1/ent3-1* double mutants showed a greatly reduced amount of cell death in the roots after AC and even DAC treatment (Supplementary Figure S7). The only exception was *smc6b-1 zrs1-4* that was hypersensitive to DAC similarly to WT plants (Supplementary Figure S6). Resistance of *zrs1-4* to 5-FUrd and AC suggests that it is a weaker modifier allele. Based on this, we conclude that *ENT3* transports also AC and DAC across the plasma membrane into the plant cells.

Hence, *ZRS1/ENT3* transports synthetic, frequently toxic, nucleosides from the AC group into *Arabidopsis* root cells. Importantly, the genetic elimination of *ENT3* protects plants against the cytotoxic effects of these drugs. In conclusion, the mapping of *ENT3* was logical but did not directly indicate the type of DNA damage induced by zebularine.

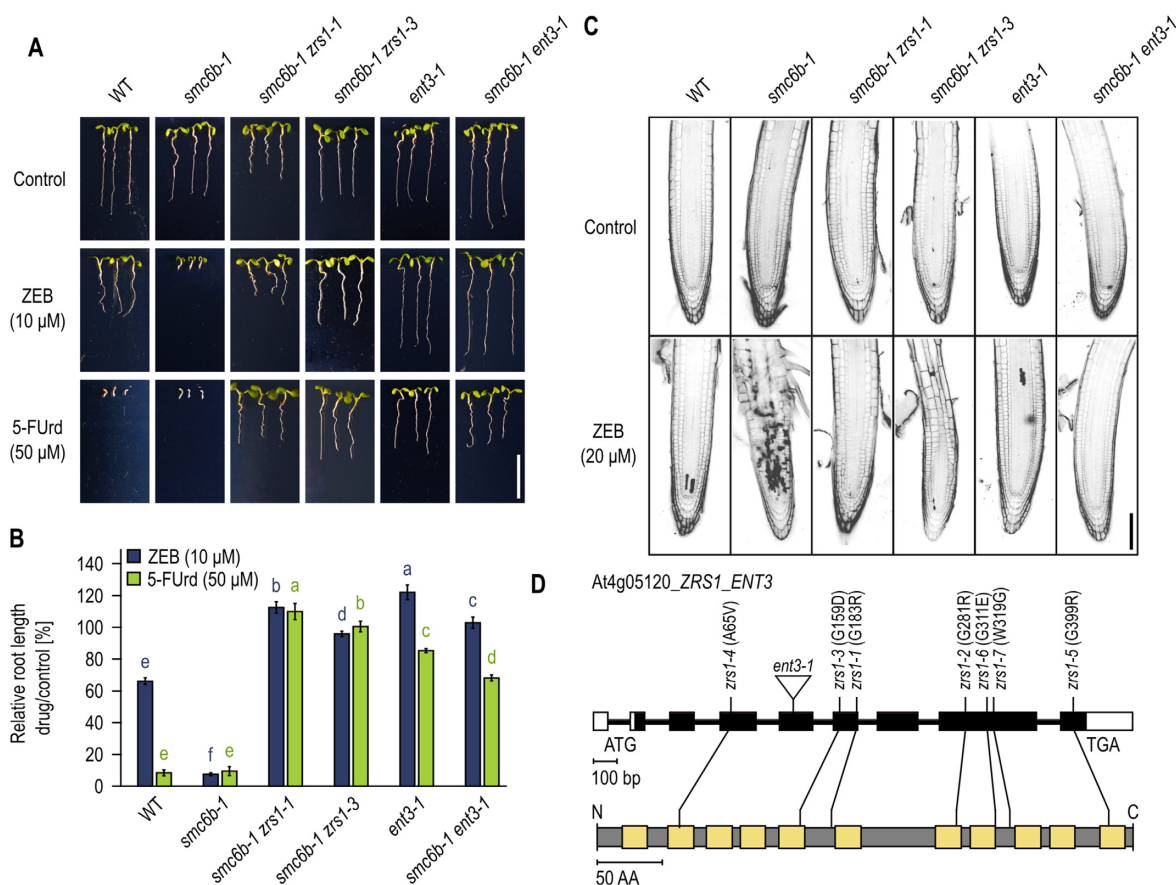


Figure 1. *ZRS1* encodes *EQUILBRATIVE NUCLEOSIDE TRANSPORTER 3 (ENT3)*. (A) Representative plants grown for 8 days on the control, 10 μ M zebularine (ZEB)- and 50 μ M 5-FUrd-containing media. Scale bar, 1 cm. (B) Quantitative data of root length. Error bars represent standard deviation between the means of three biological replicates, each with 19–35 plants. Values marked with the same letter and color do not differ according to Tukey's test ($P < 0.05$). Note: Original experiment was split between panels (A) and (B) and Supplementary Figures S3B and C and S6A and B. Therefore, both show identical images and data for the controls. (C) Representative patterns of cell death in the PI-stained roots. Five-day-old seedlings were transferred to control conditions (mock) or zebularine (20 μ M) for 48 h and then stained. Scale bar, 100 μ m. (D) Schematic gene (top) and protein (bottom) models of *ZRS1/ENT3* (At4g05120) with the positions of individual mutations and their effects on amino acids (AA). Yellow boxes in the ENT3 protein model represent transmembrane helices.

Loss of *ZRS2/DDMI* suppresses sensitivity to zebularine

Searching for suppressor mutants on 20 μ M zebularine-containing media revealed exclusively *zrs1* alleles. We hypothesized that any other potential suppressor mutations must be lethal or have a weaker phenotype, and were missed under the stringent 20 μ M zebularine selection. Therefore, we reduced zebularine concentration to 7.5 μ M for further screening. Using this strategy, we identified candidates falling into the *ZRS2* to *ZRS5* complementation groups. The confirmed candidates were further analyzed on 10 μ M zebularine.

The *smc6b-1 zrs2-1* mutant plants showed little improved root growth but had vigorously growing cotyledons that were indistinguishable from those of WT plants on 10 μ M zebularine-containing media (Figure 2A and B; Supplementary Figure S8A). The candidate had also significantly larger cotyledons on 50 μ M 5-FUrd, but the short root disqualified it as a potential *zrs1* candidate (Figure 2A and B). We crossed *smc6b-1 zrs2-1* with the nonmutagenized *smc6b-1*, developed the BCF₂ population and performed MBS,

which localized *ZRS2* to the telomere-proximal region at the bottom arm of chromosome 5 (Supplementary Figures S8B and S9). The most prominent high-effect mutation in this region was G→A change resulting in a loss of splice acceptor site at the beginning of exon 13, corresponding to the helicase C-terminal domain, in *DDMI* (At5g66750) gene (Figure 2C). To assess the effect of this splice mutation on the *DDMI* transcript, we PCR-amplified the region between exons 11 and 14 from *zrs2-1* cDNA. Surprisingly, we obtained two products that were isolated and Sanger sequenced (Supplementary Figure S10A). The more abundant (lower molecular weight) transcript *zrs2-1.1* was based on an alternative splice site in exon 13, causing a 7-bp deletion at the beginning of exon 13 and leading to a premature stop codon (Supplementary Figure S10B). The less abundant transcript *zrs2-1.2* retained the whole intron 12 (+103 nt) resulting in a premature stop codon shortly after the end of exon 12 (Supplementary Figure S10B). This confirms that *zrs2-1* carries a loss-of-function mutation in the *DDMI* gene.

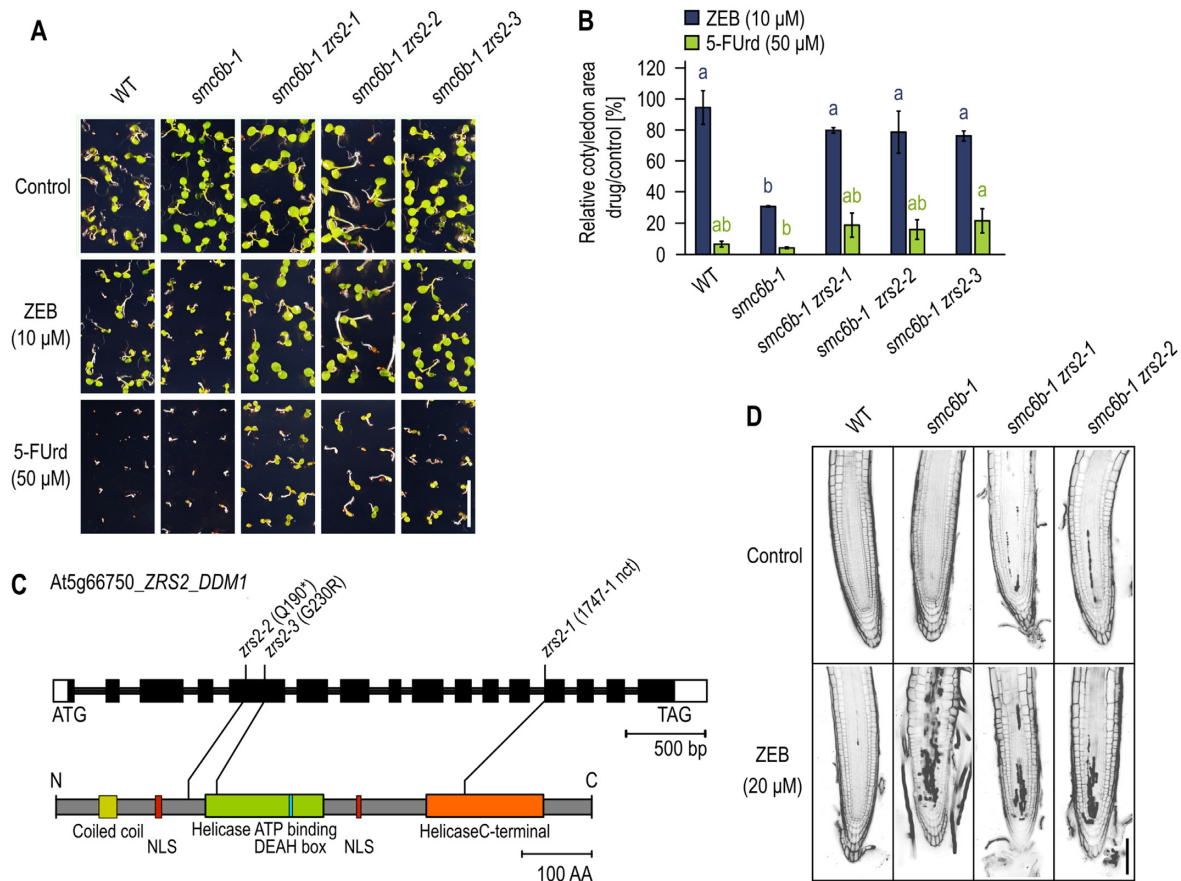


Figure 2. *ZRS2* encodes chromatin remodeling factor *DDM1*. (A) Representative cotyledon phenotypes of WT, *smc6b-1* and *smc6b-1 zrs2-1*, *zrs2-2*, *zrs2-3* seedlings grown for 8 days on control condition, 10 μ M zebularine (ZEB)- and 50 μ M 5-FUrd-containing media. Scale bar, 1 cm. (B) The relative cotyledon area was calculated as a cotyledon area per plant under drug/control conditions. Error bars represent the standard deviation of the mean between three biological replicates, each with 16–30 plants. Values marked with the same letter and color did not differ in Tukey's test ($P < 0.05$). *Note:* Original experiment was split between panels (A) and (B) and Supplementary Figure S15A and B. Therefore, both show identical images and data for the controls. (C) Gene (top) and protein (bottom) models of *ZRS2/DDM1* (At5g66750) with the positions of individual mutant alleles. nct, nucleotide in CDS; NLS, nuclear localization signal; AA, amino acids. (D) Analysis of zebularine-induced cell death. The plants were grown for 5 days on control media, treated with control conditions or 20 μ M zebularine for 48 h and then stained with PI. Scale bar, 100 μ m.

DDM1 is a well-known SWI2/SNF2-type chromatin remodeling factor involved in the maintenance of DNA methylation in all sequence contexts at repetitive sequences (11,15,46). Because *DDM1* mutations show trans-generational epigenetic inheritance effects (29,47), it is difficult to test for allelic mutations by genetic complementation. Instead, we searched for additional potential *ddm1* alleles by Sanger sequencing *DDM1* in all non-*zrs1* candidates. Using this strategy, we identified two other lines carrying a mutation in *DDM1* and thus falling into the *ZRS2* complementation group (Figure 2C). The *smc6b-1 zrs2-2* plants carried Q190* mutation. The *smc6b-1 zrs2-3* line carried a Q230R mutation directly at the conserved catalytic site of the DEAD-box helicase domain. The loss of *DDM1* function was further validated by DNA methylation analysis of the centromeric and 5S rDNA repeats using Southern analysis after digestion of genomic DNA with methylation-sensitive restriction enzymes (Supplementary Figure S11). Indeed, all three *zrs2* alleles showed a greatly reduced amount of DNA methylation in CG and CHG contexts.

The *smc6b-1 zrs2-2* plants appeared subjectively more massive compared to all other genotypes. An abnormally large body and organ size are typical signatures of polyploidy in *Arabidopsis* (48). Therefore, we analyzed the *smc6b-1 zrs2-2* ploidy by flow cytometry and found that this line is tetraploid (Supplementary Figure S10C). We measured ploidy in offspring of *smc6b-1* single mutant plants ($n = 103$) and did not find any tetraploids (F. Yang and A. Pecinka, unpublished results). Hence, the observed polyploidization event could be a spontaneous event, an effect of EMS mutagenesis, of *ddm1* mutation or of *smc6b-1 zrs2-2* double mutation.

It has to be noted that the suppressor phenotype of *smc6b-1 zrs2* plants was much weaker than that of *smc6b-1 zrs1* plants. In particular, the growth of the roots was only poorly improved compared to *smc6b-1* plants (Supplementary Figure S8A). This prompted us to analyze zebularine-induced cell death. While both WT and *smc6b-1* plants showed expected low and high amounts of dead cells, respectively, the *smc6b-1 zrs2-1* and *smc6b-1 zrs2-2* plants had an intermediate phenotype (Figure 2D), which supported

the role of DDM1 in formation of zebularine-induced DNA damage.

Here, we conclude that functional ZRS2/DDM1 is required for induction of zebularine-induced DNA damage, most likely through its heterochromatin remodeling activity.

Mapping of ZRS4 reveals MET1 as another factor required for induction of zebularine-induced DNA damage

The *smc6b-1 zrs4-1* candidate was 5-FUrd hypersensitive, but did not contain any mutation in the ZRS2/DDM1 locus by Sanger sequencing (not shown). In contrast to the previous candidates, the MBS signal was 'noisier', with many mutations of lower confidence and frequency in the repeat-rich (peri)centromeric regions (Supplementary Figure S12B). However, by stringent filtering for the high-confidence and high-frequency mutations, we localized the candidate region to the bottom arm of chromosome 5. In this region, we observed G→A nucleotide transition (100% frequency in the mapping population) leading to the A730T substitution in MET1 (At5g49160) (Figure 3C; Supplementary Figure S13). Comparison of the protein sequences from MET1 and its orthologs revealed that the *zrs4-1* mutation was on the edge of the conserved bromo-adjacent homology 1 (BAH1) domain (Supplementary Figure S14A). This domain is responsible for protein-protein interactions (49). Similar to the analysis of ZRS2, we screened the remaining candidates for possible mutations in MET1 using Sanger sequencing. One of the lines (consequently named as *smc6b-1 zrs4-2*) contained G→A nucleotide transition causing a Q863E mutation at the same BAH1 domain (Figure 3C; Supplementary Figure S14A). To test the strength of *zrs4* mutations, we performed Southern analysis after digestion with HpaII and MspI DNA methylation-sensitive enzymes and using centromeric and 5S rDNA repeats as probes (Supplementary Figure S11). This revealed DNA demethylation in the *smc6b-1 zrs4-2* plants in CG context of centromeric repeats and CHG context of 5S rDNA repeats. In contrast, there was no obvious DNA demethylation at the analyzed repeats in the *smc6b-1 zrs4-1* plants. This indicates that both identified *zrs4* alleles are hypomorphic and *zrs4-1* possibly fully decouples DNA methylation and crosslink formation processes. PI staining in the roots of double mutant plants revealed a reduced amount of dead cells compared to *smc6b-1* (Figure 3D).

Surprisingly, we did not map any other DNA methyltransferase in our screen. To test a potential suppressive role of the second replication-coupled maintenance DNA methyltransferase CMT3, we generated *smc6b-1 cmt3* double mutant, which was tested on zebularine. The *smc6b-1 cmt3* plants showed a strongly sensitive *smc6b-1*-like phenotype (Supplementary Figure S14B and C), suggesting that CMT3 does not contribute to zebularine-induced DNA damage.

Because MET1 and DDM1 genetically interact within the transcriptional gene silencing maintenance pathway (11), obtaining both genes in our suppressor genetic screen strongly suggested that their functions are needed for the zebularine-induced DNA damage.

Mutations in DDM1 and MET1 partially suppress cytotoxic effects of AC and DAC

AC and DAC are cytidine analogs structurally and functionally similar to zebularine causing also not only partial DNA demethylation but also DNA damage. Therefore, we tested whether their DNA damaging effects also depend on DDM1 and MET1. To this end, we grew *smc6b-1 zrs2* and *smc6b-1 zrs4* on media containing 10 μM AC and 5 μM DAC for eight days. The double mutants showed partially restored root growth on AC and no improvement on DAC (Supplementary Figure S15A and C), which resembled their phenotypes on zebularine. Therefore, we focused on the cotyledon area phenotypes. Here, we observed WT-like cotyledons, indicating rescue, in *smc6b-1 zrs2* and *smc6b-1 zrs4* plants under AC treatment. For the DAC treatment, only *smc6b-1 zrs2-2* (tetraploid line) showed WT-like cotyledon area, while the rest of the lines were significantly smaller than the WT but significantly larger than *smc6b-1* (Tukey's test, $P < 0.05$; Supplementary Figure S15B and D). Staining for cell death using PI revealed a lower number of dead cells in the meristematic zone of *smc6b-1 zrs2* and *smc6b-1 zrs4* plants after AC treatment, while there was no clear improvement after the DAC treatment (Supplementary Figure S15E). This reflects the results of the root length assay.

These results suggest that *zrs2* and *zrs4* mutations partially rescue *smc6b-1* growth on AC and DAC, and that MET1 and DDM1 are indeed required for the formation of AC- and DAC-induced DNA damage in *Arabidopsis*.

Zebularine, AC and DAC induce MET1 foci preferentially in 45S rDNA chromocenters

Certain types of lesions are marked by specific proteins and can be microscopically detected. To test whether this is the case for zebularine-induced DNA damage, we used translational fusion reporter line MET1-RFP (*ProMET1::MET1:RFP*) (30) and performed live-cell microscopy imaging on roots. Without zebularine (control treated with mock), we observed almost exclusively dispersed MET1-RFP nuclear signals and distinct foci could be found only in 0.4% and 2.1% of nuclei in the root apical meristem (MER) and the root elongation zone (ELO), respectively (Figure 4A). However, after 2 h treatment with 40 μM zebularine, prominent MET1-RFP foci were found in 13.0% MER and 22.9% ELO nuclei, representing 30- and 10-fold significant increases over the mock-treated control, respectively (ANOVA, post-hoc Tukey's test, $P < 0.05$; Figure 4B). To test whether the MET1 foci are induced by any type of DNA damage, we repeated the experiment using 20 μM mitomycin C and 100 nM bleomycin (Supplementary Figure S16A and B). The frequency of MET1-RFP foci was 5.2- and 5.5-fold significantly increased after these treatments in the MER zone but not in the ELO zone (Supplementary Figure S16B). Next, we analyzed the frequency of MET1-RFP foci after the treatment with AC and DAC, which revealed a 40- and 43-fold increase, respectively (Supplementary Figure S16A and B).

Based on the known role of MET1 and DDM1 in transcriptional gene silencing (29,50), we hypothesized that MET1 may act downstream of DDM1 during the formation of zebularine-induced DNA damage. This was tested

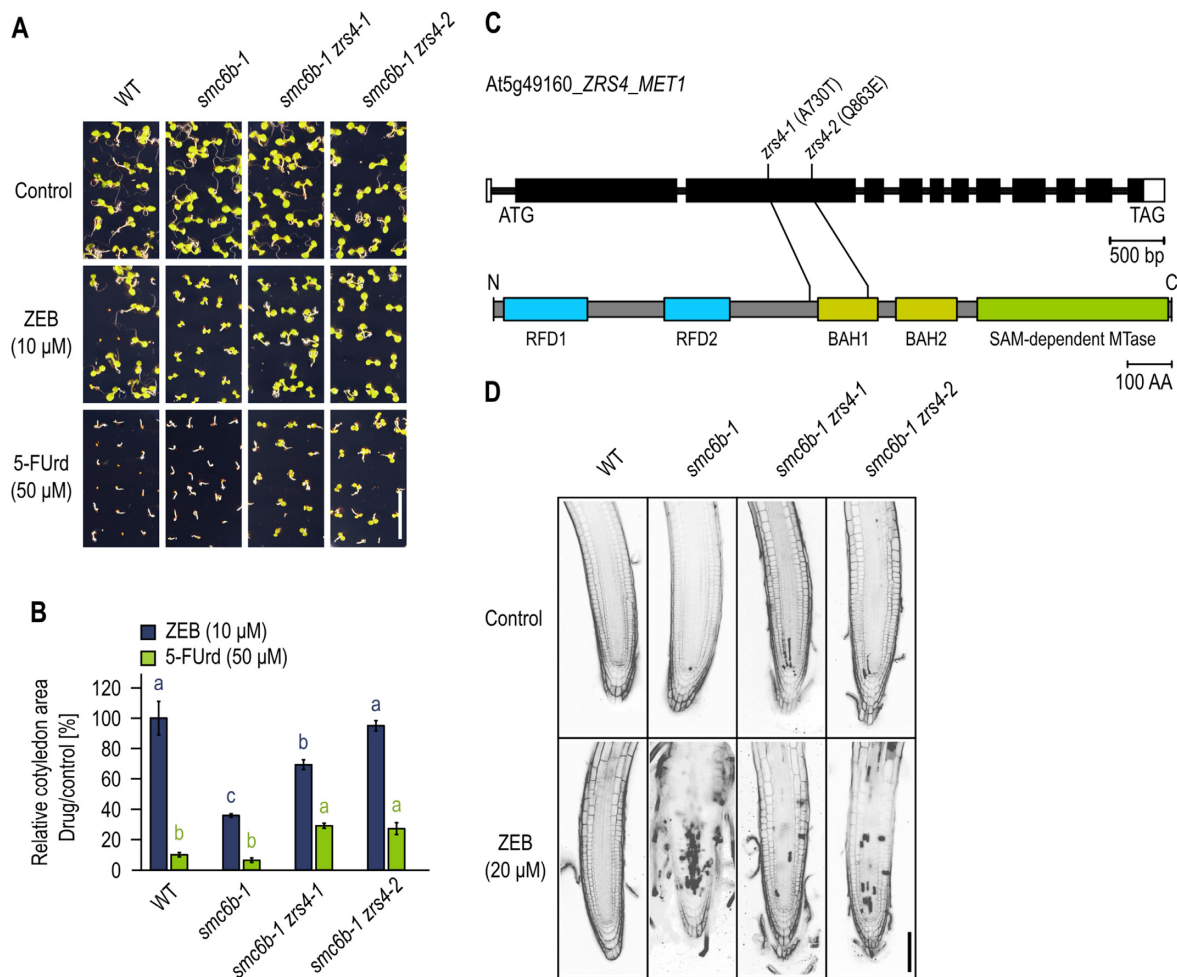


Figure 3. *ZRS4* encodes *MET1*. (A) Representative root and cotyledon phenotypes. WT and mutant plants were grown for 8 days on control, zebularine (ZEB)- and 5-FUrd-containing media. Scale bar, 1 cm. (B) The relative cotyledon area was calculated for each genotype under drug/control conditions. Error bars represent the standard deviation of the mean between three biological replicates with 19–30 plants per replicate. Values marked with the same letter and color do not differ according to Tukey's test ($P < 0.05$). Note: Original experiment was split between panels (A) and (B) and Supplementary Figure S15C and D. Therefore, both show identical images and data for the controls. (C) Gene (top) and protein (bottom) model of *ZRS4/MET1* (At5g49160) with the position of two *zrs4* alleles. RFD, replication fork domain; BAH, bromo-adjacent homology domain; AA, amino acids. (D) PI staining of 7-day-old seedlings. The seedlings were grown for 5 days on $\frac{1}{2}$ MS medium plates, and then moved to 20 μ M zebularine for 48 h and analyzed. Scale bar, 100 μ m.

by zebularine treatment of *MET1*-RFP *ddm1-5* double homozygous plants. After 8- and 24-h 40 μ M zebularine treatment, microscopic analysis revealed 54% and 90% root nuclei with *MET1*-RFP foci in the WT (*DDM1*), respectively (Figure 4C; Supplementary Figure S16D). In contrast, the zebularine-treated *MET1*-RFP *ddm1* samples contained ~13% nuclei with *MET1*-RFP foci, irrespective of the treatment length, which was significantly less than that in the WT background (ANOVA, post-hoc Tukey's test, $P < 0.05$). This strongly supports our hypothesis that *MET1* acts downstream of *DDM1* during DNA damage induced by zebularine.

In human cells, *MET1* moves along DNA attached to the PROLIFERATING CELL NUCLEAR ANTIGEN (PCNA) DNA clamp (51). Microscopic analysis of mammalian cancer cells carrying the dual reporters for GFP-Dnmt1 (animal ortholog of plant *MET1*) and RFP-PCNA revealed colocalization of both fluorescently tagged proteins under the mock conditions (52,53). Af-

ter the treatment with DAC, the GFP and RFP signals separated, indicating that PCNA continues moving forward, while *MET1* becomes crosslinked via a covalent bond with DAC to given chromosomal position. This type of DNA damage is characterized as enzymatic DPC (6). To test whether this holds true in plants, we generated line with two markers, namely *MET1*-RFP and *PCNA1*-GFP (*ProPCNA1::PCNA1-GFP*) (31). In *Arabidopsis*, *PCNA1*-GFP shows dispersed signals from G1 until early G2 and then localization to chromocenters (CCs) in late G2 (31). In the *PCNA1*-GFP *MET1*-RFP line, we observed nuclei showing several patterns: without foci, single *MET1*-RFP foci, single *PCNA1*-GFP foci and colocalized foci of both reporters (Supplementary Figure S16E). We quantified the amount of single and colocalized RFP- and GFP-containing foci in the root nuclei in mock- and zebularine-treated samples. This revealed reduction in overlap of RFP and GFP signals from 12% to 4.8% in the root meristematic zone, and from 27.4% to 16.4% in the ELO zone after zebu-

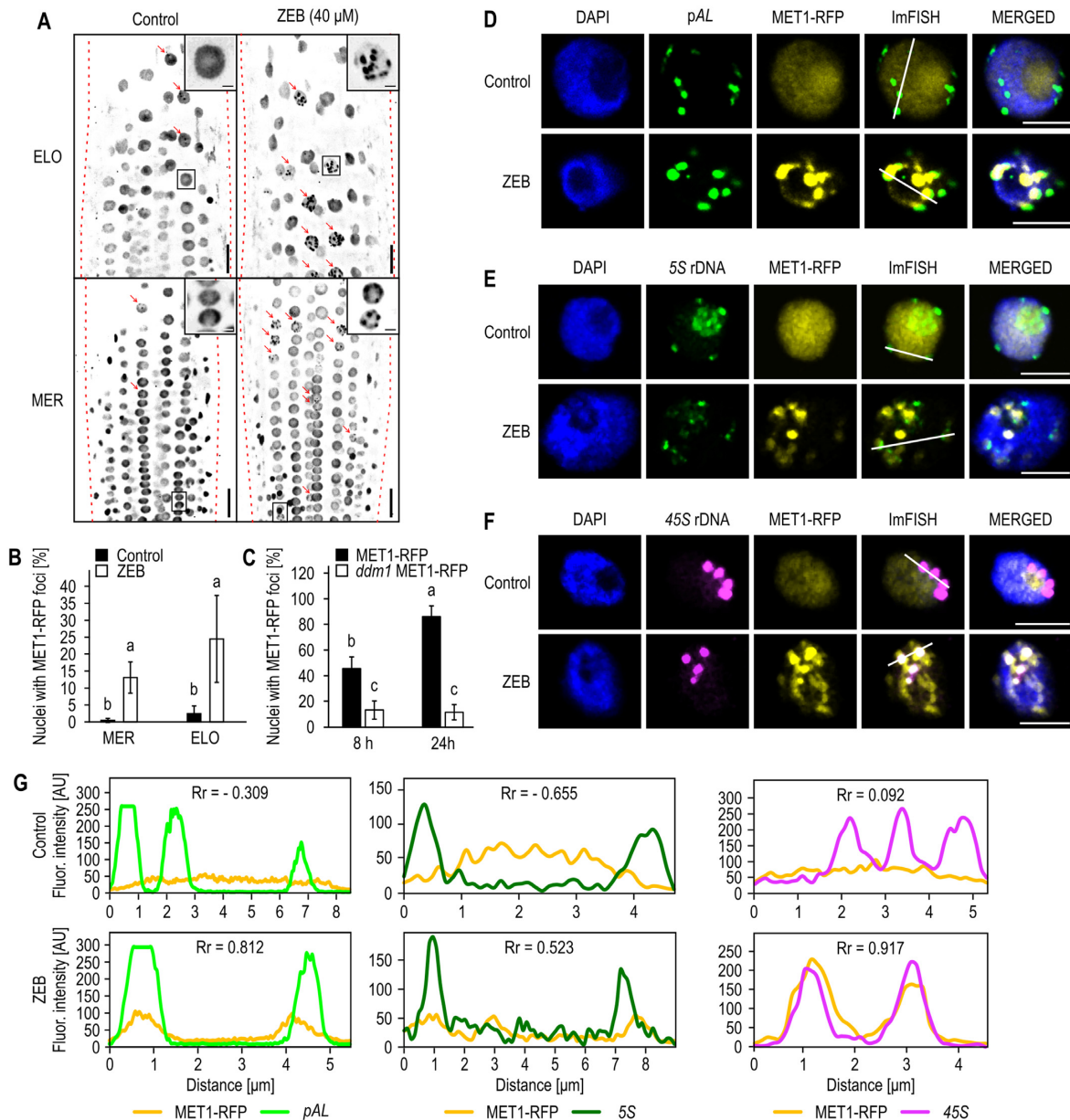


Figure 4. Zebularine-dependent formation of MET1-RFP foci in heterochromatin. **(A)** *In vivo* localization of MET1-RFP in the nuclei of control roots treated with mock (control) or 40 μ M zebularine (ZEB) for 2 h in the meristematic (MER) and the elongation (ELO) root zones of 5-day-old seedlings. Red arrows indicate nuclei with MET1-RFP foci and dashed red lines edges of the roots. The original color was converted into grayscale and inverted. Insets show typical nuclei without foci (control) and with foci (in ZEB). Scale bars, 20 μ m (main) and 3 μ m (inset). *Note:* Original experiment was split between panels (A) and (B) and Supplementary Figure S16A and B. Therefore, both show identical images and data for the controls. **(B)** Percentage of nuclei with MET1-RFP foci. Data were collected from four to five roots, containing 133–241 nuclei per root. Error bars show standard deviations between respective analyzed roots. Statistical significance of measurements in the respective zones was tested with one-way ANOVA and post-hoc Tukey’s test ($P < 0.05$). The same letters indicate samples that do not show significant differences. **(C)** Quantification of nuclei with MET1-RFP foci from roots after 8 and 24 h of 40 μ M zebularine treatment. Data were collected from five roots, containing 23–65 analyzed nuclei per root. The statistics was performed as described in panel (B). Immunofluorescence (ImFISH) of control and zebularine-treated roots for MET1-RFP (yellow) and heterochromatic loci: **(D)** centromeric repeat *pAL* (green), **(E)** 5S (green) and **(F)** 45S (magenta) rDNA. Nuclei were counterstained with DAPI. Scale bar, 5 μ m. **(G)** Fluorescence intensity plots (y-axis; arbitrary units, AU) showing the quantified colocalization of MET1-RFP signal with signal for respective heterochromatic region. The quantified area is highlighted by a white line placed in merged photo of panels (D)–(F). Rr displays Pearson’s colocalization coefficient (Rr < 0: no colocalization; $0 \leq Rr \leq 1$: the closer to 1, the stronger colocalization).

larine treatment (Supplementary Figure S16F). This suggests that in *Arabidopsis* there is a dissociation of MET1 from the PCNA clamp after zebularine treatment.

Finally, it remained unclear whether the MET1-RFP foci colocalize with specific nuclear subdomains. The overall appearance and position of these foci resembled well-known heterochromatic CCs. To test for the possible overlap, we performed co-immunostaining for MET1-RFP and the CC-specific modification H3K9me2. Under mock conditions, H3K9me2 formed a typical pattern of CCs and MET1-RFP showed a dispersed signal without any clear colocalization, as indicated by the negative Pearson correlation values (Supplementary Figure S17A and B). After zebularine treatment, MET1-RFP formed foci, some of which indeed overlapped with the H3K9me2 foci (Supplementary Figure S17C and D). This stimulated us toward more detailed analysis based on immunoFISH with probes for the centromeric repeats (*pAL*), *45S* and *5S rDNA*, i.e. the major constituents of *Arabidopsis* CCs (Figure 4D–G; Supplementary Figures S18–S20). There was no obvious colocalization between dispersed MET1-RFP and the repeat signals under mock treatment conditions. However, we observed moderate colocalization of MET1-RFP foci with *pAL* and *5S rDNA* repeats and very prominent colocalization with *45S rDNA* repeats after zebularine treatment.

Hence, zebularine induces large MET1-RFP foci, which colocalize with *45S rDNA* heterochromatic CCs and to a minor extent with other CCs. Analysis of MET1 and PCNA colocalization indicates that part of MET1 pool becomes immobilized after zebularine treatment.

Zebularine induces enzymatic DPCs with MET1

Taken together, our genetic and microscopic data suggest that zebularine-induced DNA damage is, at least in part, accompanied by enzymatic DPCs with MET1. To test this hypothesis, we performed three independent assays using 24-h mock- and 40 μ M zebularine-treated 5-day-old MET1-RFP seedlings. Our immunoFISH experiments suggested minor and major colocalization of zebularine-induced MET1-RFP foci with *5S rDNA* and *45S rDNA* CCs, respectively. This allowed us to perform direct testing for the presence of DPCs in a locus-specific manner by N-ChIP directly after the 24-h zebularine treatments with 0, 48 and 144 h of recovery at zebularine-free conditions. The N-ChIP is a modification of regular ChIP without a crosslinking followed by shearing the DNA by sonication. In this setup, only strong DNA–protein interactions are recovered. PCR analysis of ChIP DNA recovered from mock- and zebularine-treated seedlings indicated a significant enrichment ($0.15 \pm 0.001\%$ at *45S rDNA* and $0.11 \pm 0.0002\%$ at *5S rDNA* loci of zebularine-treated sample compared to $0.006 \pm 0.001\%$ at *45S rDNA* and $0.002 \pm 0.0003\%$ at *5S rDNA* loci of mock-treated sample) of MET1-RFP association with the *45S* and *5S rDNA* arrays upon zebularine treatment compared to mock-treated sample directly after 24-h zebularine treatment (Figure 5; Supplementary Figure S21). N-ChIP enrichment for MET1-RFP at target loci (*45S* and *5S rDNA*) was significantly greater than that for the IgG negative control, indicating some MET1-RFP binding to DNA even without zebularine treatment, possibly during DNA replication. During recovery, the MET1-

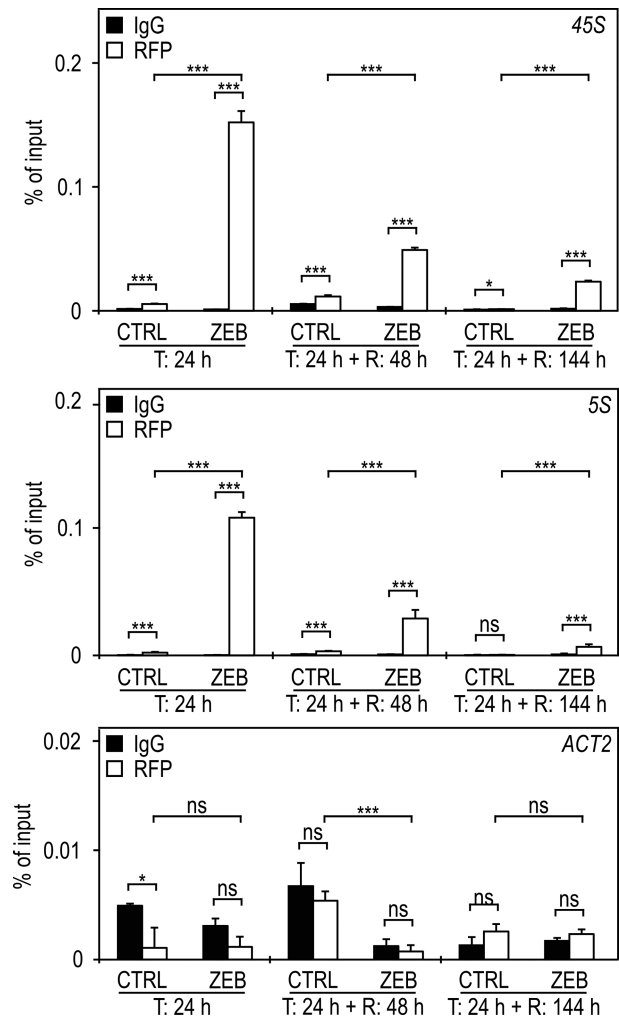


Figure 5. Zebularine induces DPCs with MET1. N-ChIP followed by qPCR was used to quantify binding of MET1-RFP using anti-RFP antibody at *45S rDNA* and *5S rDNA*. Binding to a nontarget locus (*ACT2*) was evaluated to analyze binding specificity. *Arabidopsis* seedlings were treated (T) as mock (CTRL) or with 40 μ M zebularine (ZEB) for 24 h with 0, 48 and 144 h of recovery (R) at zebularine-free conditions. Significance was determined by comparing IgG and MET1-RFP signals within the same experimental point and also between control and zebularine-treated samples. *** $P < 0.001$, * $P < 0.05$, ns = $P > 0.05$. Error bars indicate standard deviation of three technical replicates. Another biological replicate is provided in Supplementary Figure S21.

RFP peaks decreased, suggesting an ongoing repair process of the DPCs. However, the full recovery was not reached even after 1 week. As negative control, *ACT2* locus was used and no significant binding of MET1-RFP over IgG was observed at this genomic region.

Importantly, the N-ChIP provided a direct evidence that zebularine induces enzymatic DPCs with MET1 in *Arabidopsis*.

DISCUSSION

In the plant research, zebularine is used as a DNA demethylating agent with great chemical stability (17). However, it has relatively high cytotoxicity (17,54). We connected this cytotoxicity with zebularine-induced DNA damage and showed that specific DNA repair mutants are hypersensitive

to this drug (24,25). Nevertheless, the type of zebularine-induced DNA damage remained unclear. Here, we reconstructed the pathway necessary for DNA damage induction in *Arabidopsis* and provide genetic, microscopic and biochemical evidence that at least part of the damage is represented by enzymatic crosslinks between MET1 DNA methyltransferase and zebularine-containing DNA.

After administration, zebularine is actively transported into the plant cells through the activity of the ENT3 nucleoside transporter (Figure 6A and B). The *ENT3* loss-of-function mutants were frequently identified as fully resistant to zebularine in our screen. ENT3 transports also other (often toxic) cytidine analogs as demonstrated by the resistance of its mutants to 5-FUrd, AC and DAC. Surprisingly, zebularine, AC and DAC treatments even significantly enhanced the root growth of *smc6b-1 zrs1* plants compared to mock treatment. The underlying mechanism of this stimulation is currently unknown. Out of the eight *Arabidopsis* ENTs, only *ENT3* is strongly expressed in the root tissues (55). Its closest homolog *ENT6* is expressed in leaves and siliques, which possibly explains why we identified ENT3, in spite of the likely redundant biochemical function of both (or even more) family members.

Inside cells, zebularine is metabolically activated in a complex way (56). Our data suggest that at least part of the zebularine pool forms deoxyzebularine *in planta*. The fact that we did not identify any cytidine metabolic mutants is probably due to their lethality or presence of functionally redundant copies. A good example is the RIBONUCLEOTIDE REDUCTASE (RNR) complex, where *Arabidopsis* mutants in the large subunit RNR1 develop poor pale leaves (57). If viable, such plants would not show a resistance phenotype under zebularine treatment. In contrast, the small RNR subunit *RNR2A* is functionally redundant with its paralog *TSO2* and their double mutant is early somatic lethal (58).

The candidates that guided us toward DPCs were the two well-known transcriptional gene silencing factors MET1 and DDM1. Both double mutants *smc6b-1 zrs2/ddm1* and *smc6b-1 zrs4/met1* showed partial rescue phenotype and reduced amount of cell death in response to zebularine treatments. The MET1 homologs in animals and bacteria are known to form stable DNA–protein complexes with DNA containing DAC (59). *In vitro* study, using bacterial CG DNA methyltransferase *M.SssI* and zebularine-containing oligonucleotides, indicated that such complexes can be induced also by zebularine (60). Based on this, we hypothesized that MET1 molecules are trapped by zebularine-containing DNA and form enzymatic DPCs in *Arabidopsis* (Figure 6C). This was confirmed by N-ChIP assays. The main genomic regions accumulating most of the zebularine-induced DPCs are *45S rDNA* arrays. Moreover, the microscopy showed that most of the DPCs are induced to a minor extent at centromeric repeats and *5S rDNAs*. Importantly, this is consistent with the critical role of MET1 and DDM1 in maintaining high levels of DNA methylation and transcriptional repression at these genomic regions (11).

In the background of *zrs2* and *zrs4* mutants, the events leading to the formation of DPCs are strongly reduced or compromised. In the *zrs4/met1* plants, zebularine is incorporated into DNA, but the DPCs will not be formed due to

the absence of MET1 (Figure 6D). *MET1* mutations lead to misregulation of specific genes, mobilization of transposable elements and have severe effects on *Arabidopsis* development and genome stability (61,62). Both *zrs4/met1* alleles found in our screen carry amino acid substitutions linked with the BAH1 domain that is proposed to mediate protein–protein interactions. Therefore, we speculate that our *MET1* mutant alleles fail to establish specific protein–protein interaction(s). Surprisingly, the *zrs4-1* allele showed the presence of CG and CHG DNA methylation at the centromeric and *5S rDNA* repeats. The *zrs4-2* allele showed partial CG DNA demethylation of centromeric repeats and *5S rDNA*. This indicates that both *zrs4* alleles are hypomorphic.

To our knowledge, DDM1 or its orthologs have not yet been associated with the formation of enzymatic DPCs. DDM1 is an evolutionary conserved SWI2/SNF2-type chromatin remodeling factor responsible for the maintenance of CG, CHG and to a smaller extent CHH DNA methylation in a heterochromatic context in *Arabidopsis* (8). Its exact molecular function remains a matter of debate. It has been proposed to cooperate with the replication-coupled maintenance DNA methyltransferases, including MET1, to grant their access to the nucleosomal DNA in the heterochromatic context (11). More recently, DDM1 was proposed as a loader of plant-specific heterochromatic variant histone H2A.W (63). Here, we propose that although functional MET1 is present in *zrs2/ddm1* plants, it cannot reach zebularine-containing heterochromatic DNA and form toxic DPCs (Figure 6D). In a broader sense, our experiments place MET1 downstream of DDM1.

While the *zrs2/ddm1* and *zrs4/met1* mutations prevent the formation of DPCs, they should not affect the incorporation of zebularine (or other cytidine analogs) into DNA. Such incorporated analogs will still represent a threat to genome stability due to their altered chemical properties and/or lower chemical stability. However, because the damage site is not covered by the large MET1 protein (172.4 kDa), it will be accessible to other DDR pathways. Previously, we have shown that mutants in base excision and nucleotide excision repair genes are hypersensitive to AC and DAC treatments (25). Though these mutants were not sensitive to zebularine, we have observed hypersensitivity of mutant in the structure-specific endonuclease MUS81. This indicates that the incorporated zebularine, AC and DAC molecules not engaged in DPCs are repaired by other repair pathways

By the nature of MET1 as the maintenance DNA methyltransferase, we propose that the formation of zebularine-induced DPCs occurs during DNA replication. In mammals, DNMT1 is pulled on newly replicated dsDNA by the PCNA1 DNA clamp (51). After the addition of azacytidine, the colocalization of PCNA and MET1 was compromised and the latter formed stable foci that did not progress with the PCNA signal (52). Our microscopic analysis revealed that AC, DAC and zebularine induced MET1-RFP foci in *Arabidopsis* root nuclei. Importantly, these DDM1-dependent foci were specific to the MET1 enzymatic crosslinkers and not to general DNA damage-inducing agents. Remarkably, the foci were relatively large and could not represent single DPCs. Based on the immunostaining using transcription repressive modification

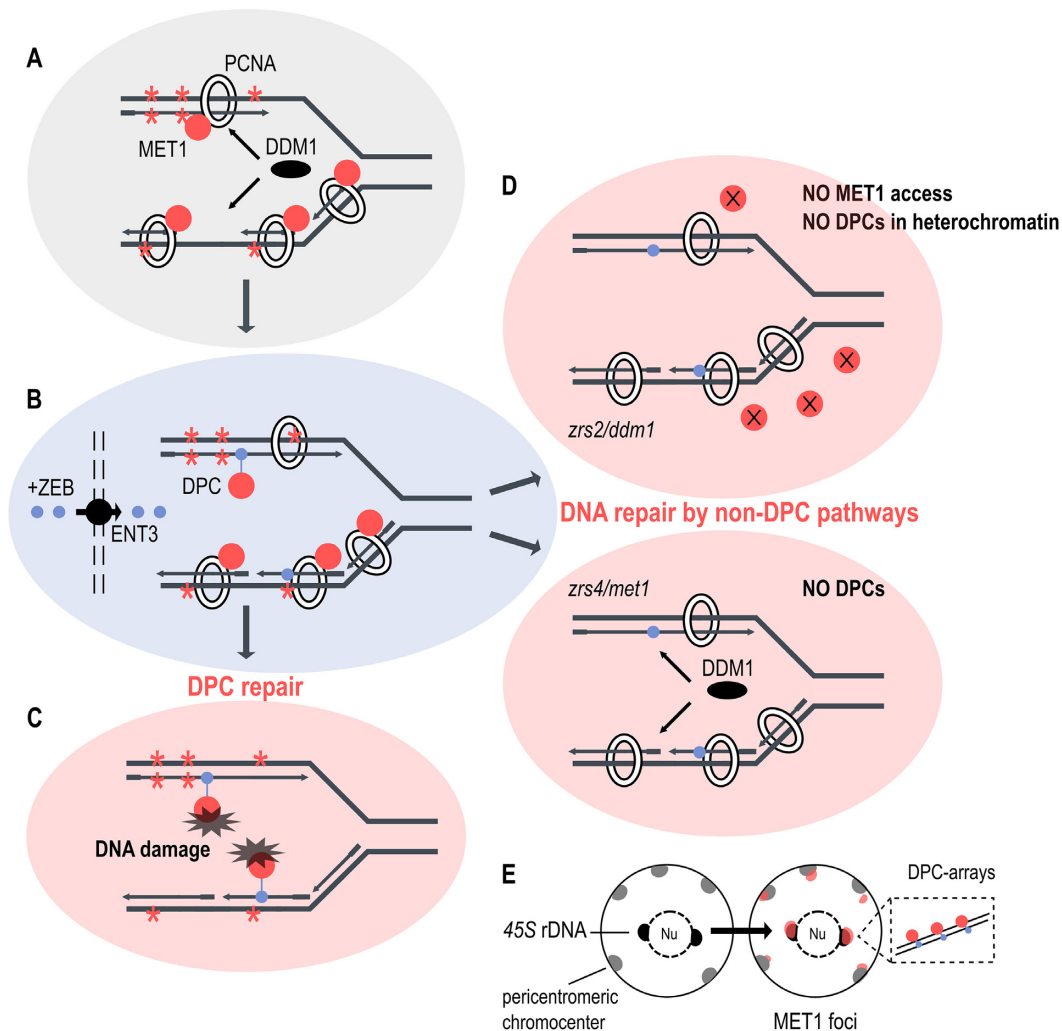


Figure 6. Working model of DNA protein crosslink formation by zebularine. (A) During DNA replication, MET1 (red sphere) in the complex with PCNA1 (double circle), and other enzymes (not shown), copies CG cytosine methylation (red asterisk) onto newly synthesized DNA strands. MET1 activity is DDM1 (black oval) dependent in heterochromatic regions. (B) Externally supplied zebularine (blue dot) is transported to the cells by the nucleoside transporter ENT3 (black circle), presumably converted into the deoxyzebularine and incorporated into a newly synthesized DNA. Replication-coupled MET1 covalently binds to zebularine, thus leading to the formation of an enzymatic DPC. (C) The DPCs trigger DNA damage repair signaling and are repaired. (D) Situation in the DPC suppressor mutants. In *zrs2/ddm1* plants, MET1 is present, but cannot methylate heterochromatic regions without functional DDM1, which prevents the formation of DPCs. In *zrs4/met1* plants, MET1 is not available and therefore no MET1-zebularine DPCs can be formed. In both scenarios, zebularine is integrated into DNA but processed by other than DPC repair pathways. (E) Schematic drawing on *Arabidopsis* nucleus showing the distribution of zebularine-induced DPCs. Heterochromatic CCs are shown as gray or black ovals and zebularine-induced MET1-RFP foci as red ovals. The DPCs accumulate in heterochromatin, particularly *45S rDNA*, possibly in a form of arrays (inset).

H3K9me2, we found that they correspond to heterochromatic CCs, in particular the ones corresponding to rDNA loci (Figure 6E). Although the organization of DPCs on chromatin is not known, we speculate that they may form arrays (Figure 6E). Currently, it is unclear whether the zebularine-induced DPCs accumulate at CCs due to the greater amount of CG DNA methylation or slower DNA damage repair in heterochromatin.

Recently, DPCs gain much attention after the discovery of a family of Wss1/Spartan proteases dedicated to their repair (3). The pioneering study revealed that this pathway is at least partially conserved in plants (4), but a deeper insight into the DPC repair in plants is so far missing. At least four types of DNA protein crosslinks can be distinguished based

on their structure, size, presence of DNA strand breaks and possibly other factors (5,6). Entrapment of DNA methyltransferases by cytidine analogs probably represents a type of DPC without DNA strand breaks. This is supported by our observation that zebularine treatment does not increase the frequency of single- or double-strand breaks (24). How are zebularine DPCs repaired is not known. We have found that SMC5/6 complex, DNA damage signaling by ATM and ATR, and homologous recombination seem to be essential in this process (24,25), but the exact mechanism is unclear and will be the focus of our future studies.

In conclusion, our study provided new insight into the effects of cytidine analogs zebularine, AC and DAC in plants by showing that they induce enzymatic DPCs. This will al-

low more precise experimental and medical use of these drugs, and interpretation of the observed phenotypes, and also opens new possibilities toward exploring DPC repair pathways in plants and animals.

DATA AVAILABILITY

Sequencing data of mapped *zrs* candidates are available in the NCBI Sequence Read Archive under accession PRJNA727751. Mapping information of respective candidates was uploaded to the UCSC Genome Browser with the following IDs:

smc6b-1 zrs1: <http://genome-euro.ucsc.edu/s/KlaProche/smc6b%2D1%20zrs1%20candidates>

smc6b-1 zrs2-1: <http://genome-euro.ucsc.edu/s/KlaProche/smc6b%2D1%20zrs2%2D1>

smc6b-1 zrs4-1: <http://genome-euro.ucsc.edu/s/KlaProche/smc6b%2D1%20zrs4%2D1>

SUPPLEMENTARY DATA

Supplementary Data are available at NAR Online.

ACKNOWLEDGEMENTS

We thank B. Eilts, P. Pečínková, J. Benecke, H. Tvardíková and E. Jahnová for technical assistance, M. Said for flow sorting nuclei, Z. Bursová for plant care, F. Yang for *zrs2-2* ploidy measurement and A. Nowicka for providing probes for Southern analysis.

Author contributions: A.P., A.F. and K.P. designed the research project. A.F., H.B. and K.P. performed genetic screening. P.D. provided bioinformatics support. K.P., A.F. and E.D.T. mapped and characterized the candidates. E.D.T. performed biochemical and cytology experiments. K.P., J.F., M.O. and J.Š. performed and evaluated subcellular localization experiments using spinning disc confocal microscopy. A.P. wrote the manuscript with the help of all authors. All authors read and approved the manuscript

FUNDING

Max Planck Society [to A.P., A.F. and H.B.]; Czech Science Foundation [19-13848S to A.P.]; Czech Academy of Sciences [to A.P.]; European Regional Development Fund [CZ.02.1.01/0.0/0.0/16_019/0000827]. Funding for open access charge: European Regional Development Fund [CZ.02.1.01/0.0/0.0/16_019/0000827].

Conflict of interest statement. None declared.

REFERENCES

- Aguilera, A. and García-Muse, T. (2013) Causes of genome instability. *Annu. Rev. Genet.*, **47**, 1–32.
- Hu, Z., Cools, T. and De Veylder, L. (2016) Mechanisms used by plants to cope with DNA damage. *Annu. Rev. Plant Biol.*, **67**, 439–462.
- Stingle, J., Schwarz, M.S., Bloemeke, N., Wolf, P.G. and Jentsch, S. (2014) A DNA-dependent protease involved in DNA–protein crosslink repair. *Cell*, **158**, 327–338.
- Enderle, J., Dorn, A., Beying, N., Trapp, O. and Puchta, H. (2019) The protease WSS1A, the endonuclease MUS81, and the phosphodiesterase TDP1 are involved in independent pathways of DNA–protein crosslink repair in plants. *Plant Cell*, **31**, 775–790.
- Hacker, L., Dorn, A. and Puchta, H. (2020) Repair of DNA–protein crosslinks in plants. *DNA Repair*, **87**, 102787.
- Stingle, J., Bellelli, R. and Boulton, S.J. (2017) Mechanisms of DNA–protein crosslink repair. *Nat. Rev. Mol. Cell Biol.*, **18**, 563–573.
- Stingle, J., Bellelli, R., Alte, F., Hewitt, G., Sarek, G., Maslen, S.L., Tsutakawa, S.E., Borg, A., Kjær, S., Tainer, J.A. *et al.* (2016) Mechanism and regulation of DNA–protein crosslink repair by the DNA-dependent metalloprotease SPRTN. *Mol. Cell*, **64**, 688–703.
- Stroud, H., Greenberg, M.V.C., Feng, S., Bernatavichute, Y. V and Jacobsen, S.E. (2012) Resource comprehensive analysis of silencing mutants reveals complex regulation of the *Arabidopsis* methylome. *Cell*, **152**, 352–364.
- Matzke, M.A. and Mosher, R.A. (2014) RNA-directed DNA methylation: an epigenetic pathway of increasing complexity. *Nat. Rev. Genet.*, **15**, 394–408.
- Du, J., Zhong, X., Bernatavichute, Y. V., Stroud, H., Feng, S., Caro, E., Vashisht, A.A., Terragni, J., Chin, H.G., Tu, A. *et al.* (2012) Dual binding of chromomethylase domains to H3K9me2-containing nucleosomes directs DNA methylation in plants. *Cell*, **151**, 167–180.
- Zemach, A., Kim, M.Y., Hsieh, P.H., Coleman-Derr, D., Eshed-Williams, L., Thao, K., Harmer, S.L. and Zilberman, D. (2013) The *Arabidopsis* nucleosome remodeler DDM1 allows DNA methyltransferases to access H1-containing heterochromatin. *Cell*, **153**, 193–205.
- Gehring, M. and Henikoff, S. (2007) DNA methylation dynamics in plant genomes. *Biochim. Biophys. Acta: Gene Struct. Expr.*, **1769**, 276–286.
- Pecinka, A. and Liu, C.H. (2014) Drugs for plant chromosome and chromatin research. *Cytogenet. Genome Res.*, **143**, 51–59.
- Kovářik, A., Koukalová, B., Lim, K.Y., Matyášek, R., Lichtenstein, C.P., Leitch, A.R. and Bezděk, M. (2000) Comparative analysis of DNA methylation in tobacco heterochromatic sequences. *Chromosome Res.*, **8**, 527–541.
- Baubec, T., Dinh, H.Q., Pecinka, A., Rakic, B., Rozhon, W., Wohlrab, B., von Haeseler, A. and Mittelsten Scheid, O. (2010) Cooperation of multiple chromatin modifications can generate unanticipated stability of epigenetic states in *Arabidopsis*. *Plant Cell*, **22**, 34–47.
- Dowd, C.L., Sutch, B.T., Haworth, I.S. and Eritja, R. (2008) Incorporation of zebularine from its derivative and activity as a template-coding nucleobase. *Nucleosides Nucleotides Nucleic Acids*, **27**, 131–145.
- Baubec, T., Pecinka, A., Rozhon, W. and Mittelsten Scheid, O. (2009) Effective, homogeneous and transient interference with cytosine methylation in plant genomic DNA by zebularine. *Plant J.*, **57**, 542–554.
- Gnyszka, A., Jastrzębski, Z. and Flis, S. (2013) DNA methyltransferase inhibitors and their emerging role in epigenetic therapy of cancer. *Anticancer Res.*, **33**, 2989–2996.
- Lee, G., Wolff, E. and Miller, J.H. (2004) Mutagenicity of the cytidine analog zebularine in *Escherichia coli*. *DNA Repair*, **3**, 155–161.
- Dote, H., Cerna, D., Burgan, W.E., Carter, D.J., Cerra, M.A., Hollingshead, M.G., Camphausen, K. and Tofilon, P.J. (2005) Enhancement of *in vitro* and *in vivo* tumor cell radiosensitivity by the DNA methylation inhibitor zebularine. *Clin. Cancer Res.*, **11**, 4571–4579.
- Covey, J.M., D’Incalci, M., Tilchen, E.J., Zaharko, D.S. and Kohn, K.W. (1986) Differences in DNA damage produced by incorporation of 5-aza-2'-deoxycytidine or 5,6-dihydro-5-azacytidine into DNA of mammalian Cells. *Cancer Res.*, **46**, 5511–5517.
- Snyder, R.D. and Lachmann, P.J. (1989) Differential effects of 5-azacytidine and 5-azadeoxycytidine on cytotoxicity, DNA-strand breaking and repair of X-ray-induced DNA damage in HeLa cells. *Mutat. Res. Lett.*, **226**, 185–190.
- Cho, S., Ishii, T., Matsumoto, N., Tanaka, H. and Eltayeb, A.E. (2011) Effects of the cytidine analogue zebularine on wheat mitotic chromosomes. *Chromosome Sci.*, **14**, 23–28.
- Liu, C.H., Finke, A., Díaz, M., Rozhon, W., Poppenberger, B., Baubec, T. and Pecinka, A. (2015) Repair of DNA damage induced by the cytidine analog zebularine requires ATR and ATM in *Arabidopsis*. *Plant Cell*, **27**, 1788–1800.
- Nowicka, A., Tokarz, B., Zwyrtková, J., Dvořák, T., Tomašíková, E., Procházková, K., Ercan, U., Finke, A., Rozhon, W., Poppenberger, B., Otmar, M. *et al.* (2020) Comparative analysis of epigenetic inhibitors reveals different degrees of interference with transcriptional gene silencing and induction of DNA damage. *Plant J.*, **102**, 68–84.

26. Díaz, M., Pečinková, P., Nowicka, A., Baroux, C., Sakamoto, T., Gandha, P.Y., Jeřábková, H., Matsunaga, S., Grossniklaus, U. and Pecinka, A. (2019) The SMC5/6 complex subunit NSE4A is involved in DNA damage repair and seed development. *Plant Cell*, **31**, 1579–1597.
27. Saze, H., Mittelsten Scheid, O. and Paszkowski, J. (2003) Maintenance of CpG methylation is essential for epigenetic inheritance during plant gametogenesis. *Nat. Genet.*, **34**, 65–69.
28. Barteel, L., Malagnac, F., Bender, J., Barteel, L., Malagnac, F. and Bender, J. (2001) Arabidopsis cmt3 chromomethylase mutations block non-CG methylation and silencing of an endogenous gene. *Genes Dev.*, **15**, 1753–1758.
29. Mittelsten Scheid, O., Afsar, K. and Paszkowski, J. (1998) Release of epigenetic gene silencing by trans-acting mutations in *Arabidopsis*. *Proc. Natl Acad. Sci. U.S.A.*, **95**, 632–637.
30. Jullien, P.E., Susaki, D., Yelagandula, R., Higashiyama, T. and Berger, F. (2012) DNA methylation dynamics during sexual reproduction in *Arabidopsis thaliana*. *Curr. Biol.*, **22**, 1825–1830.
31. Yokoyama, R., Hirakawa, T., Hayashi, S., Sakamoto, T. and Matsunaga, S. (2016) Dynamics of plant DNA replication based on PCNA visualization. *Sci. Rep.*, **6**, 29657.
32. Langmead, B., Trapnell, C., Pop, M. and Salzberg, S.L. (2009) Ultrafast and memory-efficient alignment of short DNA sequences to the human genome. *Genome Biol.*, **10**, R25.
33. Langmead, B. and Salzberg, S.L. (2012) Fast gapped-read alignment with Bowtie 2. *Nat. Methods*, **9**, 357–359.
34. Cingolani, P., Platts, A., Wang, L.L., Coon, M., Nguyen, T., Wang, L., Land, S.J., Lu, X. and Ruden, D.M. (2012) A program for annotating and predicting the effects of single nucleotide polymorphisms, SnpEff: SNPs in the genome of *Drosophila melanogaster* strain w1118; iso-2; iso-3. *Fly*, **6**, 80–92.
35. Bustin, S.A., Benes, V., Garson, J.A., Hellems, J., Huggett, J., Kubista, M., Mueller, R., Nolan, T., Pfaffl, M.W., Shipley, G.L. et al. (2009) The MIQE guidelines: minimum information for publication of quantitative real-time PCR experiments. *Clin. Chem.*, **55**, 611–622.
36. Ovečka, M., Lang, I., Baluška, F., Ismail, A., Illeš, P. and Lichtscheidl, I.K. (2005) Endocytosis and vesicle trafficking during tip growth of root hairs. *Protoplasma*, **226**, 39–54.
37. Komis, G., Luptovciak, I., Ovečka, M., Samakovli, D., Šamajová, O. and Šamaj, J. (2017) Katanin effects on dynamics of cortical microtubules and mitotic arrays in *Arabidopsis thaliana* revealed by advanced live-cell imaging. *Front. Plant Sci.*, **8**, 866.
38. Dellaporta, S.L., Wood, J. and Hicks, J.B. (1983) A plant DNA miniprep: version II. *Plant Mol. Biol. Rep.*, **1**, 19–21.
39. Southern, E.M. (1975) Detection of specific sequences among DNA fragments separated by gel electrophoresis. *J. Mol. Biol.*, **98**, 503–517.
40. Kumar, S., Stecher, G., Li, M., Niyaz, C. and Tamura, K. (2018) MEGA X: molecular evolutionary genetics analysis across computing platforms. *Mol. Biol. Evol.*, **35**, 1547–1549.
41. Pecinka, A., Schubert, V., Meister, A., Kreth, G., Klatte, M., Lysak, M.A., Fuchs, J. and Schubert, I. (2004) Chromosome territory arrangement and homologous pairing in nuclei of *Arabidopsis thaliana* are predominantly random except for NOR-bearing chromosomes. *Chromosoma*, **113**, 258–269.
42. Pecinka, A., Dinh, H.Q., Baubec, T., Rosa, M., Lettner, N. and Mittelsten Scheid, O. (2010) Epigenetic regulation of repetitive elements is attenuated by prolonged heat stress in *Arabidopsis*. *Plant Cell*, **22**, 3118–3129.
43. Mozgová, I., Wildhaber, T., Liu, Q., Abou-mansour, E., Haridon, F.L., Métraux, J., Gruissem, W., Hofius, D. and Hennig, L. (2015) Chromatin assembly factor CAF-1 represses priming of plant defence response genes. *Nat. Plants*, **1**, 15127.
44. Dvořák Tomašiková, E., Hafrén, A., Trejo-Arellano, M.S., Rasmussen, S.R., Sato, H., Santos-González, J., Köhler, C., Hennig, L. and Hofius, D. (2021) Polycomb repressive complex 2 and KRYPTONITE regulate pathogen-induced programmed cell death in *Arabidopsis*. *Plant Physiol.*, **185**, 2003–2021.
45. Traub, M., Flörchinger, M., Piecuch, J., Kunz, H.H., Weise-Steinmetz, A., Deitmer, J.W., Neuhaus, H.E. and Möhlmann, T. (2007) The fluorouridine insensitive 1 (fur1) mutant is defective in equilibrative nucleoside transporter 3 (ENT3), and thus represents an important pyrimidine nucleoside uptake system in *Arabidopsis thaliana*. *Plant J.*, **49**, 855–864.
46. Jeddeloh, J.A., Stokes, T.L. and Richards, E.J. (1999) Maintenance of genomic methylation requires a SWI2/SNF2-like protein. *Nat. Genet.*, **22**, 94–97.
47. Kakutani, T., Munakata, K., Richards, E.J. and Hirochika, H. (1999) Meiotically and mitotically stable inheritance of DNA hypomethylation induced by ddm1 mutation of *Arabidopsis thaliana*. *Genetics*, **151**, 831–838.
48. De Storme, N., Zamariola, L., Mau, M., Sharbel, T.F. and Geelen, D. (2013) Volume-based pollen size analysis: an advanced method to assess somatic and gametophytic ploidy in flowering plants. *Plant Reprod.*, **26**, 65–81.
49. Liu, X., Yu, C.-W., Duan, J., Luo, M., Wang, K., Tian, G., Cui, Y. and Wu, K. (2012) HDA6 directly interacts with DNA methyltransferase MET1 and maintains transposable element silencing in *Arabidopsis*. *Plant Physiol.*, **158**, 119–129.
50. Lippman, Z., May, B., Yordan, C., Singer, T. and Martienssen, R. (2003) Distinct mechanisms determine transposon inheritance and methylation via small interfering RNA and histone modification. *PLoS Biol.*, **1**, e67.
51. Iida, T., Suetake, I., Tajima, S., Morioka, H., Ohta, S., Obuse, C. and Tsurimoto, T. (2002) PCNA clamp facilitates action of DNA cytosine methyltransferase 1 on hemimethylated DNA. *Genes Cells*, **7**, 997–1007.
52. Schermelleh, L., Haemmer, A., Spada, F., Rösing, N., Meilinger, D., Rothbauer, U., Cardoso, C.M. and Leonhardt, H. (2007) Dynamics of Dnmt1 interaction with the replication machinery and its role in postreplicative maintenance of DNA methylation. *Nucleic Acids Res.*, **35**, 4301–4312.
53. Pali, S.S., Van Emburgh, B.O., Sankpal, U.T., Brown, K.D. and Robertson, K.D. (2008) DNA methylation inhibitor 5-aza-2'-deoxycytidine induces reversible genome-wide DNA damage that is distinctly influenced by DNA methyltransferases 1 and 3B. *Mol. Cell. Biol.*, **28**, 752–771.
54. Baubec, T., Finke, A., Mittelsten Scheid, O. and Pecinka, A. (2014) Meristem-specific expression of epigenetic regulators safeguards transposon silencing in *Arabidopsis*. *EMBO Rep.*, **15**, 446–452.
55. Li, G., Liu, K., Baldwin, S.A. and Wang, D. (2003) Equilibrative nucleoside transporters of *Arabidopsis thaliana*: cDNA cloning, expression pattern, and analysis of transport activities. *J. Biol. Chem.*, **278**, 35732–35742.
56. Ben-Kasus, T., Ben-Zvi, Z., Marquez, V.E., Kelley, J.A. and Agbaria, R. (2005) Metabolic activation of zebularine, a novel DNA methylation inhibitor, in human bladder carcinoma cells. *Biochem. Pharmacol.*, **70**, 121–133.
57. Garton, S., Knight, H., Warren, G.J., Knight, M.R. and Thorlby, G.J. (2007) crinkled leaves 8—a mutation in the large subunit of ribonucleotide reductase—leads to defects in leaf development and chloroplast division in *Arabidopsis thaliana*. *Plant J.*, **50**, 118–127.
58. Wang, C. and Liu, Z. (2006) *Arabidopsis* ribonucleotide reductases are critical for cell cycle progression, DNA damage repair, and plant development. *Plant Cell*, **18**, 350–365.
59. Ghoshal, K., Datta, J., Majumder, S., Bai, S., Kutay, H., Motiwala, T. and Jacob, S.T. (2005) 5-Aza-deoxycytidine induces selective degradation of DNA methyltransferase 1 by a proteasomal pathway that requires the KEN box, bromo-adjacent homology domain, and nuclear localization signal. *Mol. Cell. Biol.*, **25**, 4727–4741.
60. Champion, C., Guianvarc'h, D., Sénamaud-Beaufort, C., Jurkowska, R.Z., Jeltsch, A., Ponger, L., Arimondo, P.B. and Guieysse-Peugeot, A.L. (2010) Mechanistic insights on the inhibition of C5 DNA methyltransferases by zebularine. *PLoS One*, **5**, e12388.
61. Mathieu, O., Reinders, J., Čaikovski, M., Smathajitt, C. and Paszkowski, J. (2007) Transgenerational stability of the *Arabidopsis* epigenome is coordinated by CG methylation. *Cell*, **130**, 851–862.
62. Mirouze, M., Reinders, J., Bucher, E., Nishimura, T., Schneeberger, K., Ossowski, S., Cao, J., Weigel, D., Paszkowski, J. and Mathieu, O. (2009) Selective epigenetic control of retrotransposition in *Arabidopsis*. *Nature*, **461**, 427–430.
63. Osakabe, A., Jamge, B., Axelsson, E., Montgomery, S.A., Akimcheva, S., Kuehn, A.L., Pisupati, R., Lorković, Z.J., Yelagandula, R., Kakutani, T. et al. (2021) The chromatin remodeler DDM1 prevents transposon mobility through deposition of histone variant H2A.W. *Nat. Cell Biol.*, **23**, 391–400.